THE EFFECTS OF FLAME TEMPERATURE, PARTICLE SIZE AND EUROPIUM DOPING CONCENTRATION ON THE PROPERTIES OF Y_2O_3:Eu PARTICLES FORMED IN A FLAME AEROSOL PROCESS

A Thesis

by

HOON YIM

Submitted to the Office of Graduate Studies of
Texas A&M University
in partial fulfillment of the requirements for the degree of

MASTER OF SCIENCE

May 2009

Major Subject: Materials Science and Engineering

THE EFFECTS OF FLAME TEMPERATURE, PARTICLE SIZE AND EUROPIUM DOPING CONCENTRATION ON THE PROPERTIES OF Y_2O_3:Eu PARTICLES FORMED IN A FLAME AEROSOL PROCESS

A Thesis

by

HOON YIM

Submitted to the Office of Graduate Studies of
Texas A&M University
in partial fulfillment of the requirements for the degree of

MASTER OF SCIENCE

Approved by:

Chair of Committee,	Bing Guo
Committee Members,	Donald G. Naugle
	Xinghang Zhang
Intercollegiate Faculty Chair,	Tahir Cagin

May 2009

Major Subject: Materials Science and Engineering

ABSTRACT

The Effects of Flame Temperature, Particle Size and Europium Doping Concentration on the Properties of Y_2O_3:Eu Particles Formed in a Flame Aerosol Process. (May 2009)

Hoon Yim, B.A., Ajou University

Chair of Advisory Committee: Dr. Bing Guo

Y_2O_3:Eu particles are phosphors that have found wide applications. Flame-synthesized Y_2O_3:Eu particles may have either the cubic or the monoclinic structure. The effects of particle size and Eu doping concentration on crystal structure and the surface elemental composition of the flame-synthesized Y_2O_3:Eu particles had not been previously reported.

In this study, a flame aerosol process was used to generate polydisperse Y_2O_3:Eu particle. H_2 was used as the fuel gas, with either air or O_2 gas as the oxidizer. The precursor was aqueous solutions of the metal nitrates, atomized using a 1.7-MHz ultrasonic atomizer. The product particles were analyzed by transmission electron microscopy (TEM), X-ray diffractometer (XRD), Selected area electron diffraction (SAED), X-ray photoelectron spectroscopy (XPS), fluorescence spectrophotometer, and inductively coupled plasma mass spectrometer (ICP-MS).

The Y_2O_3:Eu particles generated in H_2/O_2 flames were spherical and fully dense, with diameters in the range of 10~3000 nm. In particle samples with lower Eu doping concentrations, a critical particle diameter was found, whose value increased with

increasing Eu doping concentration. Particles well below the critical diameter had the monoclinic structure; those well above the critical diameter had the cubic structure. At sufficiently high Eu doping concentrations, all Y_2O_3:Eu generated in H_2/O_2 flames had the monoclinic structure. On the other hand, all particles generated in the H_2/air flames had the cubic structure. For the Y_2O_3:Eu particles generated in H_2/O_2 flames, XPS results showed that the surface Eu concentration was several times higher than the doping concentration. For Y_2O_3:Eu particles generated in H_2/air flames, the surface Eu concentration was equal to the doping concentration. For both types of particles, the photoluminescence intensity reached a maximum corresponding to a surface Eu concentration 40~50%. The photoluminescence intensity then decreased rapidly with higher Eu doping concentration.

The effect of particle size and Eu doping concentration on crystal structure may be explained by the interplay between surface energy and polymorphism. A mechanism for this surface enrichment phenomenon was proposed based on the binary Eu_2O_3-Y_2O_3 phase diagram.

DEDICATION

To my parents, wife, two daughters, and all of my family members who have always been there for me

ACKNOWLEDGEMENTS

First, I would like to thank my advisor Dr. Guo. He supported and guided me for two years with enthusiasm. I would also like to express my sincere thanks to Dr. Naugle and Dr. Zhang for valuable comments and recommendations.

One of the people that gave me great help is the MSEN coordinator, Ms. Gerston. My group members are good colleagues. I was able to discuss difficult problems with them and enjoyed studying with them.

TABLE OF CONTENTS

Page

LIST OF FIGURES

LIST OF TABLES

1. INTRODUCTION

Europium-doped Y_2O_3 is a widely used red phosphor Y_2O_3:Eu, which has found applications in field emission display [1], medical imaging [2], advanced lighting, and biological labeling [3]. In Y_2O_3:Eu the Eu^{3+} ions substitute the Y^{3+} ions and emit visible fluorescence under proper excitation. One of the strongest fluorescence peaks is assigned to the $^5D_0 \rightarrow {}^7F_2$ transition of Eu^{3+} [4]. The doping concentration of Eu in Y_2O_3 is usually around 5% (atomic ratio) for typical phosphor applications [5]. Y_2O_3 has multiple crystal structures, two of which are encountered in normal synthesis processes, namely the cubic phase (space group: $Ia\bar{3}$ (206)) and the monoclinic phase (space group: C2/m(12)). The cubic phase is the stable phase of bulk Y_2O_3 at room temperature and pressure. The monoclinic phase is metastable under ambient conditions [6]. Cubic and monoclinic Y_2O_3:Eu phosphors have significantly different photoluminescence spectra [7, 8]; monoclinic Y_2O_3:Eu has lower photoluminescence intensity than cubic Y_2O_3:Eu [9, 10].

A number of methods may be used to synthesize Y_2O_3:Eu particles, including colloidal methods [11-13], combustion in fuel-oxidizer mixture [14], evaporation–condensation [15, 16], furnace spray pyrolysis [17]. Flame aerosol synthesis is able to generate ceramic oxide particles that are dense, near-spherical, non-agglomerated, with well-controlled stoichiometry [18]. Flame aerosol synthesis can be achieved in a continuous, one-step process, and is flexible in scale. In comparison to wet-chemistry and plasma methods, a recent review paper concluded that flame aerosol synthesis is more economic

---

This thesis follows the style of *Analytical Chemistry*.

for making metal oxide particles of heavier elements, complex composition and lower valence state [19]. Apparently flame aerosol synthesis may prove to be advantageous for Y_2O_3:Eu. However, there are some significant challenges in the flame synthesis of Y_2O_3:Eu particles.

One of them is the control of crystal structure and morphology. To have spherical, fully dense Y_2O_3:Eu particles, high flame temperature is necessary. Low flame temperature produces undesirable morphology, such as hollow particles [10]. However, at high flame temperatures the as-synthesized Y_2O_3:Eu particles often have the monoclinic structure, although at low flame temperature the as-synthesized Y_2O_3:Eu particles only have the cubic structure [8]. In a previous study on pure Y_2O_3 particles synthesized in high-temperature flames, Guo and Luo found a particle size effect on the crystal structure of Y_2O_3 particles. The particles had the cubic structure if they were larger than a critical size, while those smaller had the monoclinic structure [20]. This finding suggests that if one may be able to control the crystal structure of Y_2O_3 particles by controlling their size. Due to the crystalographical similarity between pure Y_2O_3 and Y_2O_3:Eu particles, one may assume that such a crystal-structure control scheme may be used for Y_2O_3:Eu particles as well. However, to assess the feasibility of this strategy, it is necessary to determine the correlation between particles size and crystal structure for Y_2O_3:Eu particles, at both high and low flame temperatures. Apparently this correlation would be dependent on the Eu doping concentration (defined as the molar ratio between Eu and total metal (Y and Eu)). On the other hand, there had been little knowledge about the distribution of Eu within a flame-synthesized Y_2O_3:Eu particle, although the

distribution of Eu may play an important role in the fluorescence behavior of micrometer-sized Y_2O_3:Eu particles. In particular, Eu concentration near the particle surface may be very important because most reactions take place on the particle surface.

Although a number of research groups have carried out research on flame aerosol synthesis of Y_2O_3:Eu particles, the photoluminescence properties of these particles as a function of synthesis conditions (e.g. flame temperature and Eu doping concentration) have not been systematically investigated [8, 9, 21].

The objective of this study is to determine the effects of flame temperature, particle size and Eu doping concentration on the crystal structure, the photoluminescence intensity, and the surface concentration of europium for Y_2O_3:Eu particles formed in a flame aerosol process.

2. METHODOLOGY

Eu-doped Y_2O_3 particles were synthesized using flame spray pyrolysis. $Y(NO_3)_3 \cdot 6H_2O$ and $Eu(NO_3)_3 \cdot 6H_2O$ aqueous solutions with various Eu/Y ratios were used. H_2/O_2(or Air) laminar diffusion flames were used for flame spray pyrolysis. X-ray diffraction and selected area electron diffraction were used to determine the crystal structure of the particle samples. Photoluminescence was characterized by fluorescence spectroscopy. Surface and overall chemical compositions of the particles were measured by X-ray photoelectron spectroscopy and inductively coupled plasma mass spectroscopy.

2.1 Precursor solution preparation

The precursor solutions were prepared by dissolving yttrium nitrate hexahydrate (chemical formula: $Y(NO_3)_3 \cdot 6H_2O$, Alfa Aesar, Ward Hill, MA) and europium nitrate hexahydrate (chemical formula: $Eu(NO_3)_3 \cdot 6H_2O$, Alfa Aesar, Ward Hill, MA) into Nanopure® water (Barnstead, Dubuque, IO). The total molar concentration of the precursor solution was maintained at approximately 0.76M, while the Eu doping concentration (defined as the atomic ratio of Eu to total metals in the precursor) was varied from 2.5% to 25%. The conditions of the precursor solutions are listed in Table 1.

Table 1. Precursor solution and flame conditions.

Samples (Eu %)	Mole concentration	Molar ratio		Flame condition	
		Y	Eu	Fuel	Oxidizer
Y_2O_3:Eu(2.5%)	0.77M	0.975	0.025	H_2 (1 SLM)	O_2 (6 SLM)
Y_2O_3:Eu(5%)	0.77M	0.950	0.050	H_2 (1 SLM)	O_2 (6 SLM)
Y_2O_3:Eu(10%)	0.76M	0.900	0.100	H_2 (1 SLM)	O_2 (6 SLM)
Y_2O_3:Eu(15%)	0.76M	0.850	0.150	H_2 (1 SLM)	O_2 (6 SLM)
Y_2O_3:Eu(20%)	0.75M	0.800	0.200	H_2 (1 SLM)	O_2 (6 SLM)
Y_2O_3:Eu(25%)	0.75M	0.750	0.250	H_2 (1 SLM)	O_2 (6 SLM)
Y_2O_3:Eu(2.5%)	0.77M	0.975	0.025	H_2 (1 SLM)	Air (6 SLM)
Y_2O_3:Eu(5%)	0.77M	0.950	0.050	H_2 (1 SLM)	Air (6 SLM)
Y_2O_3:Eu(10%)	0.76M	0.900	0.100	H_2 (1 SLM)	Air (6 SLM)
Y_2O_3:Eu(15%)	0.76M	0.850	0.150	H_2 (1 SLM)	Air (6 SLM)
Y_2O_3:Eu(20%)	0.75M	0.800	0.200	H_2 (1 SLM)	Air (6 SLM)
Y_2O_3:Eu(25%)	0.75M	0.750	0.250	H_2 (1 SLM)	Air (6 SLM)
Y_2O_3:Eu(30%)	0.74M	0.700	0.300	H_2 (1 SLM)	Air (6 SLM)
Y_2O_3:Eu(40%)	0.73M	0.600	0.400	H_2 (1 SLM)	Air (6 SLM)
Y_2O_3:Eu(50%)	0.72M	0.500	0.500	H_2 (1 SLM)	Air (6 SLM)

2.2 Synthesis of particles

Samples were prepared by flame spray pyrolysis using H_2 diffusion flames with O_2 support and with Air support. The adiabatic flame temperature of a H_2/O_2 flame was approximately 3000K, in comparison to the approximately 2400K of a H_2/Air flame [22].

Figure 1 shows a schematic of the flame spray pyrolysis apparatus. The flame spray pyrolysis method has been described in detail elsewhere [20]. Briefly, a syringe pump fed the precursor solution into the atomizer vessel at 5 ml/h. The H_2 fuel gas flew through the vessel and carried the precursor droplets generated by atomizer into the flame through the furnace. The droplets underwent solvent evaporation and precursor decomposition to form Y_2O_3:Eu particles. The H_2 and O_2 (or Air) flow rates were kept at 1 SLM and 6 SLM respectively. The Y_2O_3:Eu particles then were collected on an alumina filter (Whatman, Maidstone, England).

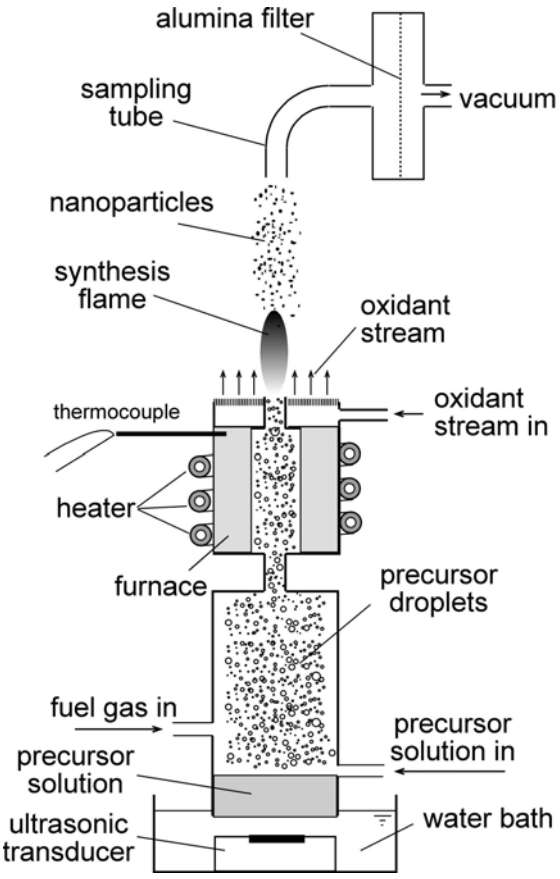

Figure 1. Schematic of flame spray pyrolysis apparatus.

2.3 Characterization of particles

Particle size distribution

The particle size distributions were obtained by surveying multiple TEM images of each sample. The diameter of a particle was measured in random orientations on the TEM micrograph. The particle size distributions in terms of number fraction in each size bin are plotted. A detailed description of procedure is given in Appendix A.

X-ray diffraction

The particles collected on alumina filter were directly put on the sample stage and analyzed in a Bruker-AXS D8 Powder X-ray diffractometer (Bruker, Madison, WI) with a Cu source.

Photoluminescence

A Cary Eclipse Fluorescence Spectrophotometer (Varian, Palo Alto, CA) was used for the photoluminescence measurement. In order to compare the fluorescence intensity of different samples, a reference material was required. Y_2O_3:Tb was used as the internal fluorescence reference material, whose main peaks do not overlap with that of Y_2O_3:Eu. Y_2O_3:Tb was prepared with the same method with Y_2O_3:Eu. Tb molar concentration was 2.5% with respect to Y and Tb molar concentration. The sample and the internal reference was suspended in isopropanol and dried out. Each Y_2O_3:Eu sample was mixed with the Y_2O_3:Tb reference, holding the mass ratio of Y_2O_3:Tb/Y_2O_3:Eu at

1/7. A detailed description of the procedure is given in Appendix B. The spectra were obtained using UV light and were normalized at 488nm which is the main photoluminescence peak of Y_2O_3:Tb.

Transmission electron microscopy

For the transmission electron microscopy (TEM) analysis, the Y_2O_3:Eu particles were carefully scraped off the filter and suspended in ethanol. Drops of the Y_2O_3:Eu ethanol suspension were put on 300 mesh copper grids with type-B carbon film support (Ted Pella Inc., CA). After evaporation of the ethanol, Y_2O_3:Eu particles were deposited on the grids and TEM samples were thus obtained. Transmission electron microscopy (TEM) samples were then measured in a JEOL 2010 microscope (Jeol Ltd., Tokyo, Japan) operated at 200kV. The TEM images were recorded with a Gatan ORIUS CCD camera (Gatan Inc., Pleasanton, CA).

Selected area electron diffraction

To determine the critical particle diameter, selected area electron diffraction (SAED) was used to measure the crystal structure of individual Y_2O_3 particles from 2.5% Eu-doped Y_2O_3 to 10% Eu-doped Y_2O_3 samples. With an SAED aperture of the suitable size, it was possible to gather electron diffraction signal from a single particle. In order to obtain a distinctive electron diffraction pattern, sample tilting with the aid of a double tilt holder was required. Depending on the orientation of the particle on the

TEM grid, sample tilting of up to 30˚ relative to the horizontal plane was sometimes needed.

X-ray photoelectron spectroscopy

X-ray photoelectron spectroscopy (XPS) was carried out for the particles samples in a Kratos Axis Ultra Imaging XPS (Kratos Analytical, Manchester, UK). The samples were fixed on the sample stage using copper-based scotch tape and were measured with a Al source. Surface Eu concentration (defined as the atomic ratio of Eu to total metals) was obtained based on the XPS results. The method of the analysis is described in Appendix C.

Inductively coupled plasma mass spectrometry

Inductively coupled plasma mass spectrometry (ICP-MS) was carried out for the particles samples in an ELAN DRC II mass spectrometer (Perkinelmer, Ontario, Canada). All the powder samples were digested with 0.1ml of concentrated nitric acid at 95ºC for 30 minutes. Afterwards, they were cooled and diluted to 10 ml with deionized water. Yttrium and Europium standard solutions (Inorganic ventures, Inc., Lakewood, NJ) were used in order to determine the concentration of analytes (e.g., Y or Eu) in these samples. Thus the overall Eu concentration (defined as the atomic ratio of Eu to total metals in the digested particles) was obtained.

3. RESULTS

3.1 Particle morphology and size distribution

Y_2O_3:Eu samples were synthesized in H_2 diffusion flame with O_2 support. Representative TEM image of Y_2O_3:Eu samples is shown in Figure 2. All the particles were spherical and appeared to be fully dense based on the TEM results. Using multiple TEM images of the samples, particle size distribution was obtained by counting average 600 particles. The particle size distributions are shown in Figure 3. Although 5% Eu-doped Y_2O_3 sample has slightly larger size, the Y_2O_3:Eu samples with various Eu concentration had similar particle size distributions.

Particle size statistics for the samples are shown in Table 2 and Figure 3. About 4,000 particles were measured and the mean particle size was 847nm.

It had been found that, with decreasing precursor concentration, the as-synthesized particle diameter decreased [20]. It is very natural that the Eu doping concentration had no effect on particle size. It was shown in Table 2 and Figure 3.

In contrast to particles generated form the H_2/O_2 flames, those generated from H_2/air flames had irregular shapes. Most of them also appeared to be hollow [18]. Particle size distribution was measured for 2.5% Eu-doped Y_2O_3, as shown in Table 2 and Figure 3. The mean particle size, 1110 nm, was larger than that of the samples prepared in H_2/O_2 flame. It is because most of the particle was hollow.

(a)

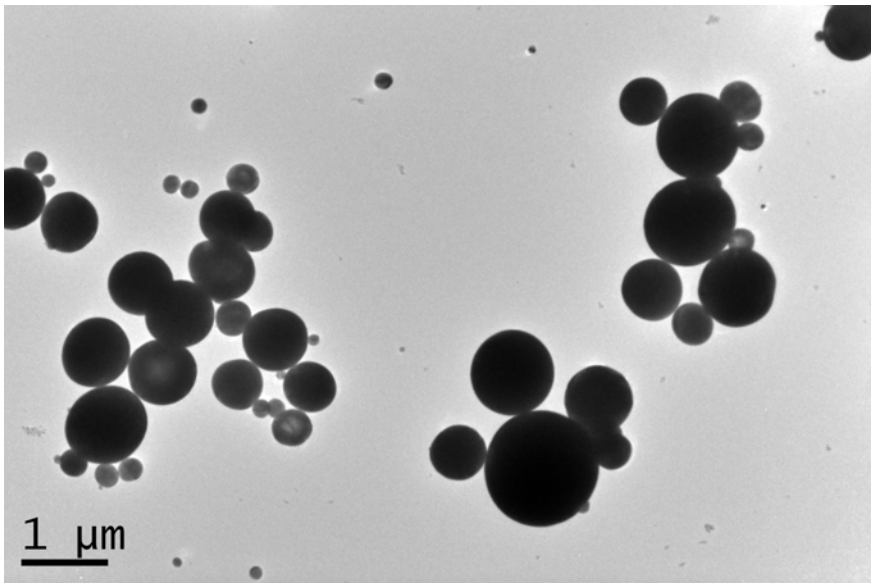

(b)

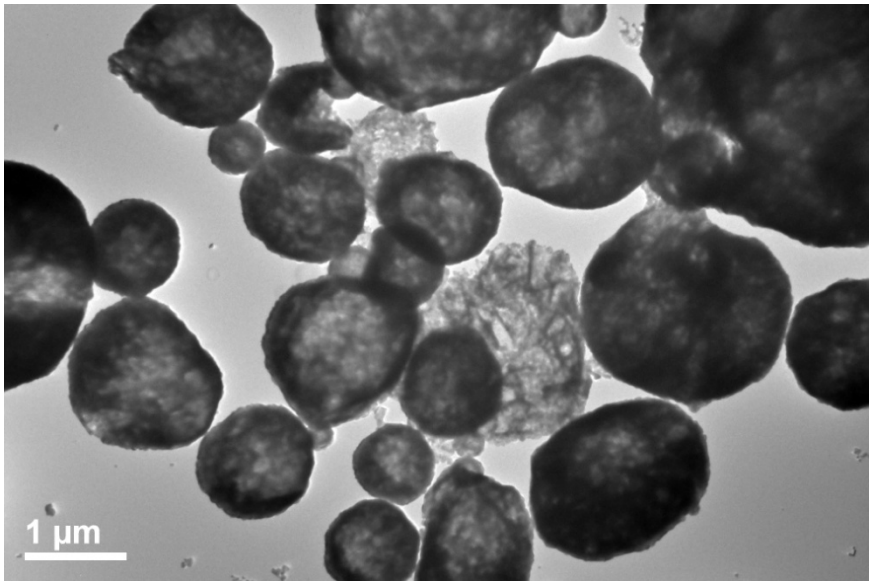

Figure 2. Representative TEM images of 2.5% Eu-doped Y_2O_3:Eu. (a) was synthesized at H_2/O_2 flame, and (b) was synthesized at H_2/Air flame.

Table 2. Particle size statistics for the samples with various Eu doping concentrations. (a) All samples listed were prepared at H_2 flame with O_2 support. (b) Sample was prepared in H_2 flame with Air support.

(a)

Samples (Eu %)	Mean Size (nm)	Median Size (nm)	Maximum size (nm)	Minimum size (nm)	Standard Deviation (nm)	Number of Particles Measured
Y_2O_3:Eu(2.5%)	727	724	1800	69	290	613
Y_2O_3:Eu(5%)	995	930	2880	10	383	968
Y_2O_3:Eu(10%)	793	790	2780	80	326	1035
Y_2O_3:Eu(15%)	823	780	2970	130	353	518
Y_2O_3:Eu(20%)	827	810	1940	100	338	254
Y_2O_3:Eu(25%)	856	870	1820	190	306	547
All Samples	847	820	2970	10	349	3935

(b)

Samples (Eu %)	Mean Size (nm)	Median Size (nm)	Maximum size (nm)	Minimum size (nm)	Standard Deviation (nm)	Number of Particles Measured
Y_2O_3:Eu(2.5%)	1110	1035	3400	120	555	234

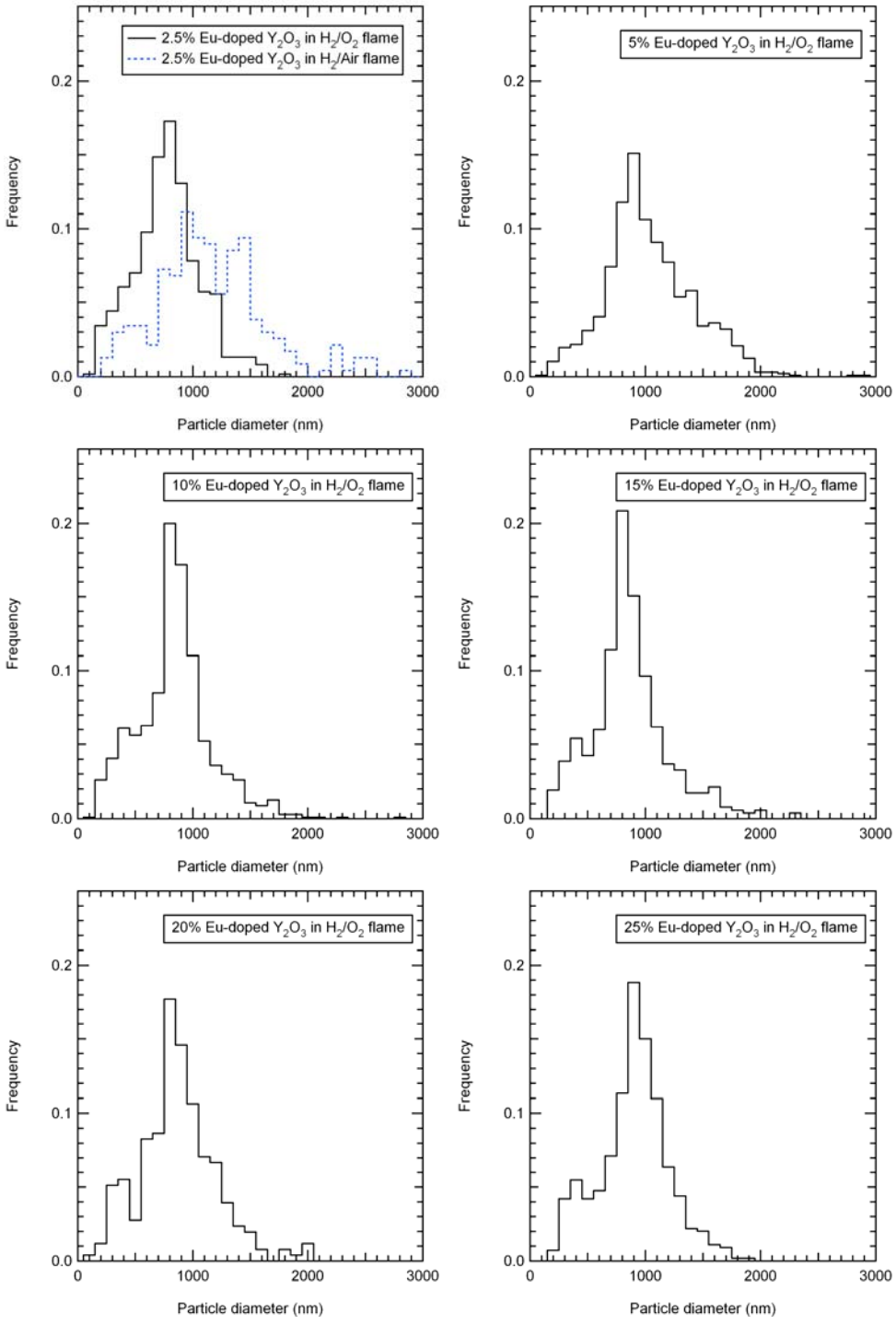

Figure 3. Particle size distribution for the samples with various Eu doping concentrations.

3.2 Powder X-ray diffraction

Figure 4 shows the representative XRD patterns of Y_2O_3:Eu samples. The patterns matched the cubic and monoclinic Y_2O_3 XRD standards PDF# 41-1105 and PDF# 44-0399. These showed that the samples contained both the cubic and the monoclinic structures. In the figure, filled diamonds indicate the strongest peak of the cubic phase. The peak intensity of the cubic phase relative to that of the monoclinic decreased with increasing Eu doping concentration. For Eu concentration higher than 15% the peaks associated with the cubic phase were absent. This suggests that the cubic fraction of the 2.5% Eu-doped Y_2O_3 sample was higher than that of the 10% Eu-doped Y_2O_3 sample and there was no more cubic structure at Eu doping concentrations higher than 15%. The results suggested that the higher the Eu concentration, the more monoclinic structure would be formed; the critical particle diameter would increase with Eu concentration. It will be discussed with SAED results and phase diagram.

(a)

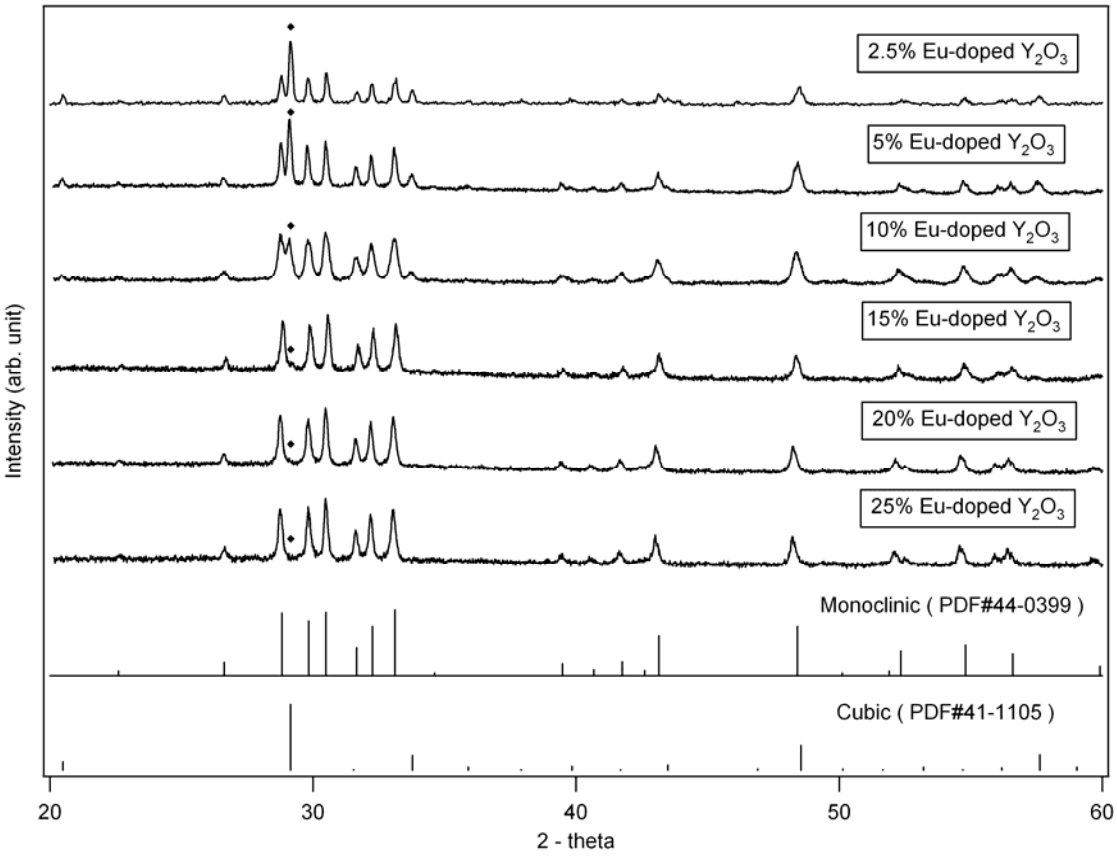

Figure 4. X-ray diffraction patterns. (a) X-ray diffraction patterns for Y_2O_3:Eu particle samples that were synthesized in H_2/O_2 flames. Filled diamonds indicate the strongest peak of the cubic phase at 2θ of 29.150º. (b) X-ray diffraction patterns for Y_2O_3:Eu particle samples that were synthesized in H_2/Air flames.

(b)

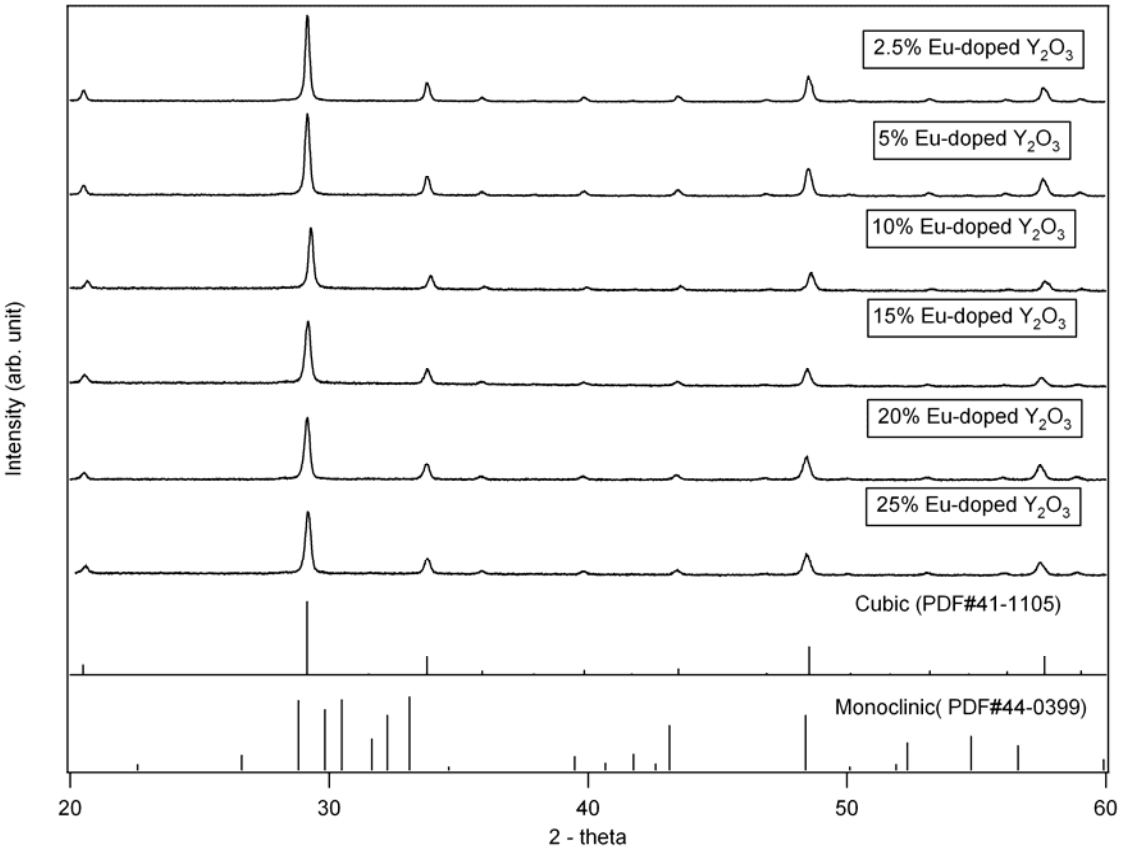

Figure 4. Continued

3.3. Single particle selected area electron diffraction

Single particle selected area electron diffraction (SAED) was employed to determine the crystal structure of individual particles. The electron diffraction results showed that the particles were single crystals, as can be seen from their spot patterns shown in Figure 5-(a). A detailed description of the SAED measurement can be found elsewhere [20]. A total of about 50 SAED measurements were carried out for each of the Y_2O_3:Eu samples. The crystal structure of each particle was then determined by comparing the diffraction pattern with the index tables that had been calculated for the monoclinic and the cubic structures of Y_2O_3. Some representative SAED patterns are shown in Figure 5-(a). The probability of a particle being monoclinic was then calculated as a function of the particle diameter. The results are shown in Figure 5-(b). The results for pure Y_2O_3 particles were adapted from Guo and Luo [20]. For pure Y_2O_3, all particles below 1.0 μm were monoclinic; those above 2.0 μm are all cubic. The

probability changes sharply with size for particles with intermediate sizes. Based on the curve fitting of the probability data, a critical particle diameter may be obtained. This is defined as the size at which the probability of the particle being either phase is 50%. The critical particle diameter of Y_2O_3:Eu samples was determined and summarized from Y_2O_3 to 10% Eu-doped Y_2O_3 in Table 3 [20]. Single particle electron diffraction was not carried out for samples with higher Eu concentrations (15%, 20%, 25% Eu-doped Y_2O_3). By extrapolation, the critical particle diameter would be approximately 2.5um, 2.8um and 3.1um for 15%, 20%, 25% Eu doping concentrations, respectively. This was in agreement with the XRD results, which showed no cubic peaks for samples with Eu doping concentrations of 15% or greater. In these range, there were very few particles to measure around the critical particle diameter. Among all measured particles, only 14 particles (0.35% 14 out of 3935) were bigger than 2μm.

Table 3. The critical particle diameter with various Eu doping concentrations.

Samples (Eu %)	The Critical Particle Diameter (μm)	Number of Particles Measured
Y_2O_3 [20]	1.5	60 >
Y_2O_3:Eu(2.5%)	1.7	60
Y_2O_3:Eu(5%)	1.9	35
Y_2O_3:Eu(10%)	2.2	30
Y_2O_3:Eu(15%)	Not measured	Not measured
Y_2O_3:Eu(20%)	Not measured	Not measured
Y_2O_3:Eu(25%)	Not measured	Not measured

(a)

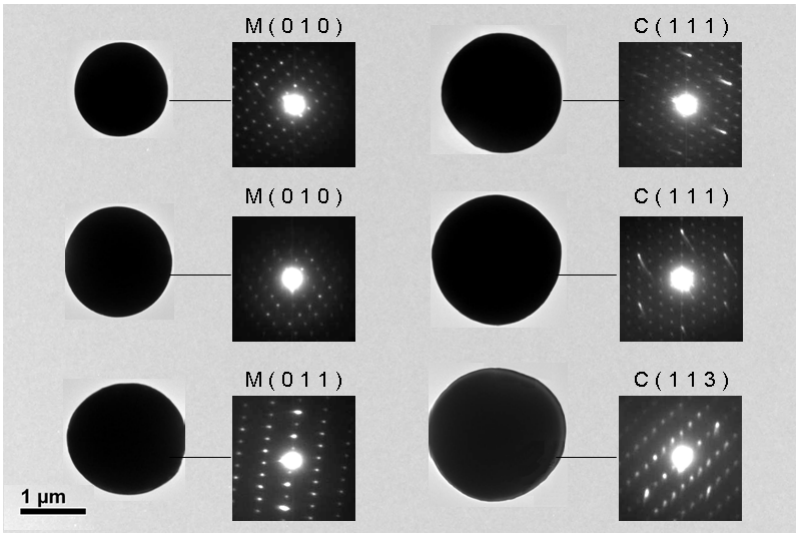

(b)

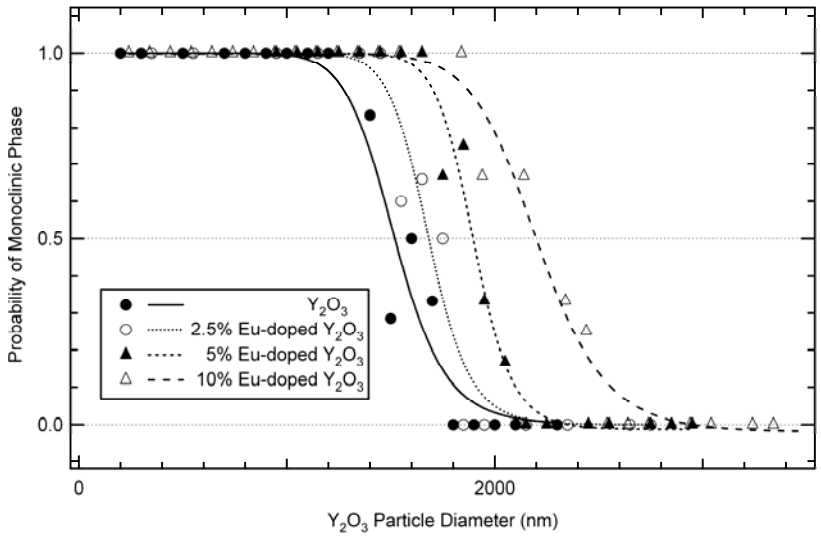

Figure 5. The critical particle diameter for Eu-doped Y_2O_3. (a) Representative SAED pattern for cubic and monoclinic. (b) Probability of particle being the monoclinic structure for the Y_2O_3:Eu samples with various Eu doping concentration. (c) The Critical particle diameter with Eu doping concentration.

(c)

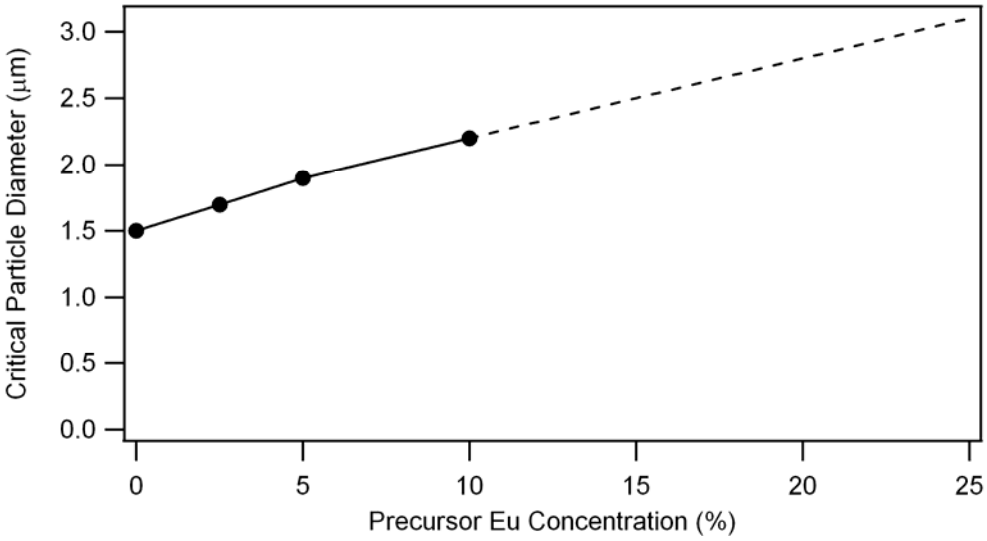

Figure 5. Continued

3.4 Photoluminescence

The photoluminescence of the Y_2O_3:Eu samples was measured for Eu concentrations from 2.5% to 25%. Figure 6 shows the photoluminescence spectra of Eu-doped Y_2O_3 samples, with an excitation wave length of 260nm. The spectra were normalized at 488nm which is one of main peak in Y_2O_3:Tb particles.

For the samples synthesized in H_2/O_2 flames, there were two main peaks found for all Y_2O_3:Eu samples, one at 615nm and the other at 624nm. For Eu concentration below 15%, the photoluminescence intensity of Y_2O_3:Eu samples increased with increasing Eu concentration. The photoluminescence intensity then drops rapidly after 20% Eu-doped Y_2O_3. The Y_2O_3:Eu sample with 15% Eu had the highest photoluminescence intensity. This result agreed well with that found by other researchers [8].

For the samples synthesized in H_2/Air flame, there were one main peak (612nm) found for all Y_2O_3:Eu samples. The photoluminescence intensity of Y_2O_3:Eu samples increased with increasing Eu concentration until the Eu concentration reached 40%. The photoluminescence intensity then decreased with increasing Eu concentration.

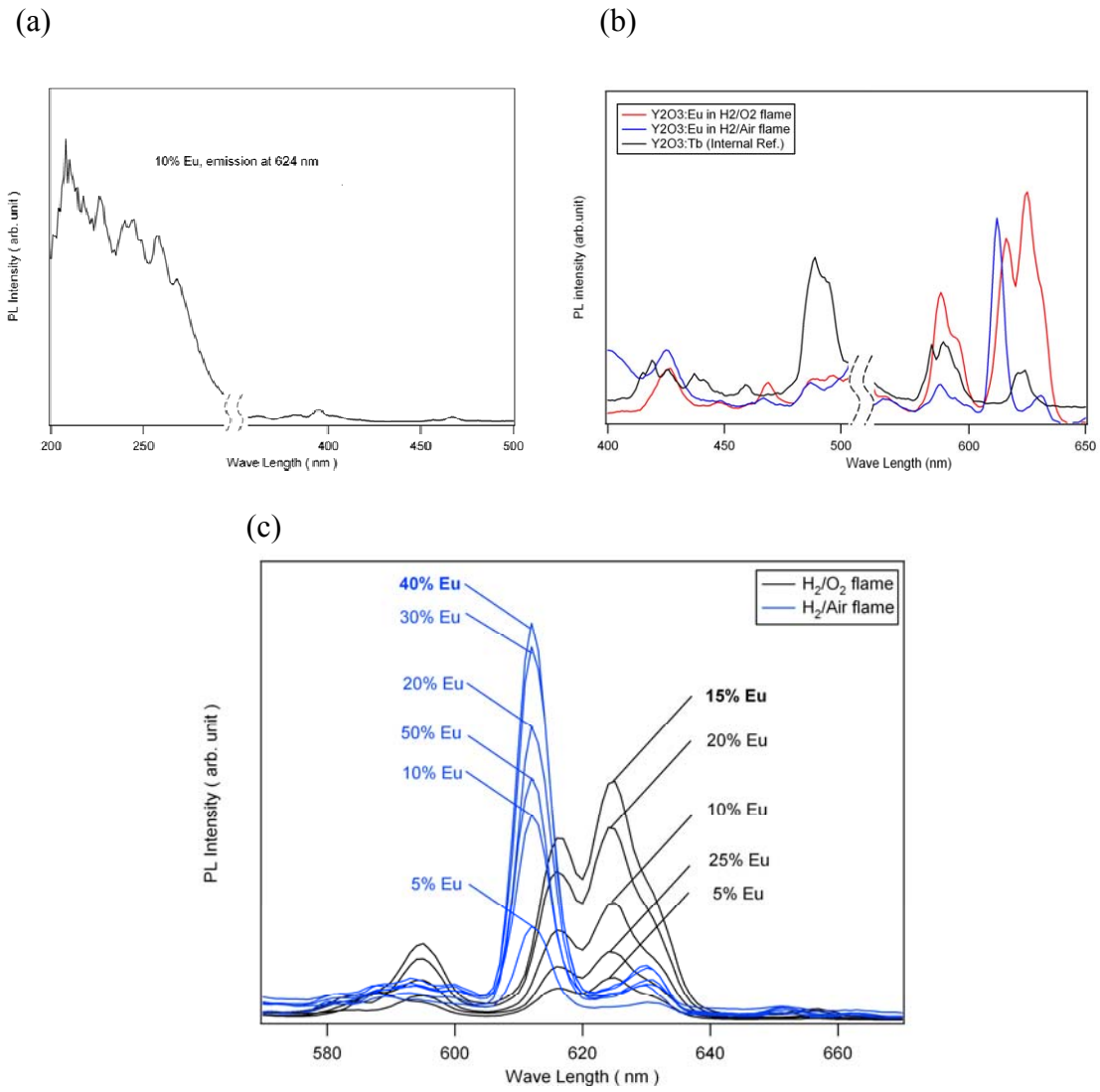

Figure 6. Photoluminescence spectrum for Eu-doped Y_2O_3. (a) PL excitation spectrum of Y_2O_3 :Eu with emission measured at 624 nm; (b) PL emission spectra of Y_2O_3:Eu samples and that of Y_2O_3:Tb which is the internal reference. (c) PL emission spectra of Y_2O_3:Eu samples. The photoluminescence spectrum were normalized to the internal fluorescence reference Y_2O_3:Tb.

3.5 X-ray photoelectron spectroscopy and inductively coupled plasma mass spectrometer

X-ray Photoelectron Spectroscopy (XPS) and Inductively Coupled Plasma Mass Spectrometer (ICP-MS) for Eu-doped Y_2O_3 were measured from 2.5% Eu-doped Y_2O_3 to 25% Eu-doped Y_2O_3. The measurement results are listed in Table 4 and Figure 7. The Eu/Y ratios measured by ICP-MS were in excellent agreement with the Eu/Y raios of the corresponding precursor solutions; during the synthesizing process, molar composition of Eu/Y did not change.

For the Y_2O_3:Eu particles prepared in H_2 flame with O_2 support, the XPS measurement results showed much higher Eu/Y ratios than the corresponding precursor Eu/Y ratios. However, for the Y_2O_3:Eu particles prepared in H_2 flames with air support, the XPS results showed the same Eu/Y ratio as that of the precursor. Surface enrichment of Eu element in Y_2O_3:Eu particles only took place in H_2 flame with O_2 support.

Table 4. The results of ICP-MS measurements and XPS measurements. (a) The samples were prepared in H_2 flame with O_2 support. (b) The samples were prepared in H_2 flame with Air support.

(a)

Samples (Eu %)	Relative Y and Eu concentrations measured by ICP-MS		Relative Y and Eu concentrations measured by XPS	
	Y	Eu	Y	Eu
Y_2O_3:Eu(2.5%)	0.975	0.025	0.880	0.120
Y_2O_3:Eu(5%)	0.951	0.049	0.804	0.196
Y_2O_3:Eu(10%)	0.903	0.097	0.560	0.440
Y_2O_3:Eu(15%)	0.848	0.152	0.518	0.482
Y_2O_3:Eu(20%)	0.790	0.210	0.336	0.664
Y_2O_3:Eu(25%)	0.754	0.246	0.311	0.689

(b)

Samples (Eu %)	Relative Y and Eu concentrations measured by ICP-MS		Relative Y and Eu concentrations measured by XPS	
	Y	Eu	Y	Eu
Y_2O_3:Eu(2.5%)	0.977	0.023	0.976	0.024
Y_2O_3:Eu(5%)	0.951	0.049	0.951	0.049
Y_2O_3:Eu(10%)	0.895	0.105	0.909	0.091
Y_2O_3:Eu(15%)	0.850	0.150	0.864	0.136
Y_2O_3:Eu(20%)	0.803	0.197	0.818	0.182
Y_2O_3:Eu(25%)	0.759	0.241	0.781	0.219

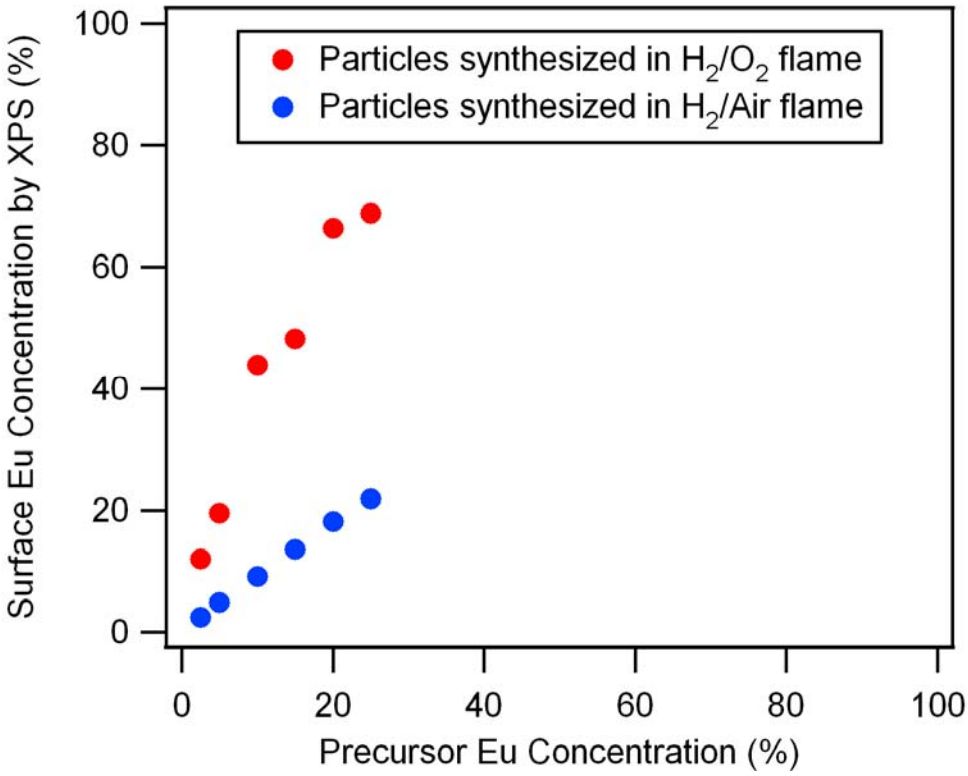

Figure 7. X-ray photoelectron spectroscopy results for Eu-doped Y_2O_3.

4. DISCUSSIONS

4.1 Surface enrichment of Eu

The adiabatic flame temperature of a H_2/O_2 flame is approximately 3000 K. Although the maximum flame temperature in an O_2 supported H_2 diffusion flame is lower than the adiabatic flame temperature, it is still very likely high enough to melt the Y_2O_3:Eu particles with Figure 8 [23]. Therefore, the Y_2O_3:Eu particles generated in H_2/O_2 flames very likely experienced a melting-solidification process in the flame. The near-spherical shape and the dense morphology of these particles were in agreement with such melting-solidification formation history.

The Eu enrichment on particle surface was probably a result of the melting-solidification process, in conjunction with the phase equilibrium characteristics of the Eu_2O_3-Y_2O_3 system.

Figure 8 is the phase diagram of the Eu_2O_3-Y_2O_3 system in air. At Eu concentration used in this study, when a molten Y_2O_3:Eu particle started to solidify, Eu would start to enrich in the remaining melt. X mole fraction liquid phase cools down and reaches T_b temperature in Figure 9. X mole fraction liquid phase then become γ mole fraction liquid and α mole fraction H phase. γ mole fraction liquid phase cools down again and reaches T_c temperature. γ mole fraction liquid phase then become δ mole fraction liquid and β mole fraction H phase. The Eu enrichment in the remaining melt would continue until the entire particle was solidified. If in the solidification process the

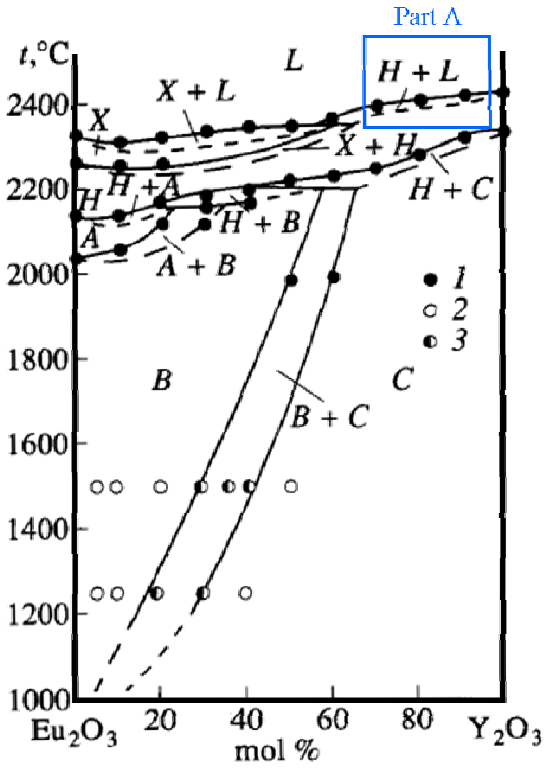

Figure 8. The phase diagram of Eu_2O_3-Y_2O_3 system [23]. Europia (Eu_2O_3) and yttria (Y_2O_3), can crystallize in any of the five well-know polymorphic forms of rare-earth oxides: monoclinic (B-phase, sp. gr. *C2/m*), two hexagonal (A-phase, sp. gr. *C3m*; H-phase, sp.gr. *$P6_3/mmc$*), and two cubic (C-phase, sp. gr. *Ia3*; X-phase, sp. gr. *Im3m*). L stands for liquid phase.

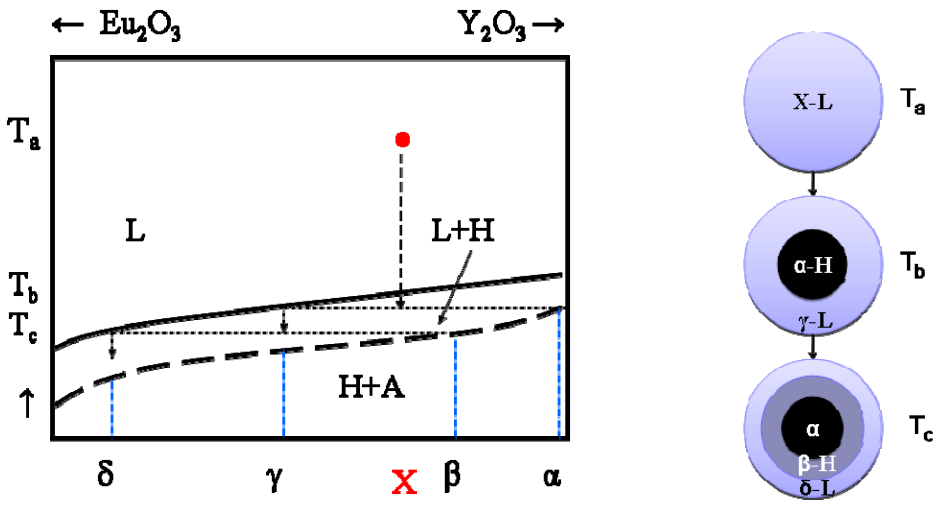

Figure 9. The phase diagram of Eu_2O_3-Y_2O_3 system at part A of Figure 8. x-axis is mole fraction, y-axis is temperature. X is mole fraction which may represent from 2.5% to 25% Eu concentration. γ and α are the mole fractions which meet the phase boundary at T_b. δ and β are the mole fractions which meet the phase boundary at T_c.

melt was on the particle surface, then the particle surface would be enriched in Eu because it would be solidified from the last remaining melt. If two phases contact each other, one phase which has lower surface energy would be on the particle surface to minimize total energy. In this case, the melt has lower surface energy since the surface energy is proportional to the melting point [24].

This phenomenon only takes place at high flame temperature process. The result of XPS for the samples shows that the Eu concentration on surface depends on the flame temperature.

4.2 Photoluminescence

Concentration quenching took place when the surface concentration of Eu approached 50%. This may be explained intuitively that, at this Eu concentration level, Eu ions began to occupy adjacent lattice point. When this happened, non-radiative energy transfer between neighboring Eu ions became highly probable, and hence concentration quenching became significant. With further increase in Eu surface concentration, the effect of concentration quenching became increasingly pronounced, and the PL intensity quickly decreased with increasing Eu concentration.

4.3 Effect of Eu doping concentration on critical diameter

In a previous study, Guo and Luo derived a relationship between the critical particle diameter and thermodynamics properties of cubic and monoclinic Y_2O_3.

$$D_{cr} = \frac{6M\gamma\left(\frac{2}{3}\frac{\Delta\rho}{\rho} - \frac{\Delta\gamma}{\gamma}\right)}{\rho(\Delta h - T\Delta s)} \quad (1)$$

where Δh and Δs are the changes in molar enthalpy and entropy; D is the diameter of the particle; γ is the specific surface energy; ρ is the density of Y_2O_3 and $\Delta\rho$ is the density change for the cubic$\rightarrow$monoclinic transition; M is the molecular mass of Y_2O_3.

Eu doping may affect all the terms in the equation. However, quantitative assessment of the doping effect on these terms is not possible at this moment. The surface enrichment of Eu further complicated the interpretation of the critical particle diameter.

5. SUMMARY AND CONCLUSIONS

- All particles synthesized in H_2/air flames had the cubic structure.
- The crystal structure of particles synthesized in H_2/O_2 flames was dependent on particle size and Eu doping concentration. The critical particle size increased with increasing Eu concentration.
- Surface enrichment of Eu was found for particles synthesized in H_2/O_2 flames. The surface Eu concentration (defined as the atomic ratio of Eu to total metal on the surface of particle) was the same as the Eu doping concentration (defined as the atomic ratio of Eu to total metal in the precursor) for particles synthesized in H_2/air flames.
- Surface enrichment of Eu might be explained with phase diagram, assuming the particles underwent melting-solidification processes in the flames.
- The photoluminescence intensity (or the integral of PL curve) reached a maximum at Eu surface concentration of 40~50%, regardless of the overall Eu concentration.

Based on the results, optimum Eu concentration could be found in the view of phase and photoluminescence characteristics; at 15% Eu concentration, the Y_2O_3:Eu particles have phase-pure monoclinic and the highest photoluminescence intensity.

Phase-pure monoclinic Y_2O_3:Eu particles may be generated by controlling Eu concentration or particle size. In a high-temperature flame, where binary metal oxide particles experience melting and solidification, one metal element may be enriched on the surface of particle depending on the binary metal oxide phase diagram. The maximum photoluminescence intensity of Y_2O_3:Eu particles occurs when the surface Eu concentration reaches 40~50%, regardless of the overall Eu concentration.

REFERENCES

(1) Cho, S. H.; Kwon, S. H.; Yoo, J. S.; Oh, C. W.; Lee, J. D.; Hong, K. J.; Kwon, S. J. ***Journal of the Electrochemical Society*** **2000**, *147*, 3143-3147.

(2) Cavouras, D.; Kandarakis, I.; Panayiotakis, G. S.; Evangelou, E. K.; Nomicos, C. D. ***Medical Physics*** **1996**, *23*, 1965-1975.

(3) Feng, J.; Shan, G. M.; Maquieira, A.; Koivunen, M. E.; Guo, B.; Hammock, B. D.; Kennedy, I. M. ***Analytical Chemistry*** **2003**, *75*, 5282-5286.

(4) Bihari, B.; Eilers, H.; Tissue, B. M. ***Journal of Luminescence*** **1997**, *75*, 1-10.

(5) Camenzind, A.; Strobel, R.; Pratsinis, S. E. ***Chemical Physics Letters*** **2005**, *416*, 193-197.

(6) Hoekstra, H. R. ***Inorganic Chemistry*** **1966**, *5*, 754-757.

(7) Dosev, D.; Guo, B.; Kennedy, I. M. ***Journal of Aerosol Science*** **2006**, *37*, 402-412.

(8) Qin, X.; Ju, Y. G.; Bernhard, S.; Yao, N. ***Journal of Materials Research*** **2005**, *20*, 2960-2968.

(9) Camenzind, A.; Strobel, R.; Krumeich, F.; Pratsinis, S. E. ***Advanced Powder Technology*** **2007**, *18*, 5-22.

(10) Kang, Y. C.; Seo, D. J.; Park, S. B.; Park, H. D. ***Japanese Journal of Applied Physics Part 1-Regular Papers Short Notes & Review Papers*** **2001**, *40*, 4083-4086.

(11) Jiang, Y. D.; Wang, Z. L.; Zhang, F. L.; Paris, H. G.; Summers, C. J. ***Journal of Materials Research*** **1998**, *13*, 2950-2955.

(12) Martinez-Rubio, M. I.; Ireland, T. G.; Fern, G. R.; Silver, J.; Snowden, M. J. ***Langmuir*** **2001**, *17*, 7145-7149.

(13) Graeve, O. A.; Corral, J. O. ***Optical Materials*** **2006**, *29*, 24-30.

(14) Kottaisamy, M.; Jeyakumar, D.; Jagannathan, R.; Rao, M. M. ***Materials Research Bulletin*** **1996**, *31*, 1013-1020.

(15) Krauss, W.; Birringer, R. ***Nanostructured Materials*** **1997**, *9*, 109-112.

(16) Skandan, G.; Hahn, H.; Parker, J. C. ***Scripta Metallurgica Et Materialia*** **1991**, *25*, 2389-2393.

(17) Kang, Y. C.; Roh, H. S.; Seo, D. J.; Park, S. B. ***Journal of Materials Science Letters*** **2000**, *19*, 1225-1227.

(18) Pratsinis, S. E. ***Progress in Energy and Combustion Science*** **1998**, *24*, 197-219.

(19) Osterwalder, N.; Capello, C.; Hungerbuhler, K.; Stark, W. J. ***Journal of Nanoparticle Research*** **2006**, *8*, 1-9.

(20) Guo, B.; Luo, Z. P. ***Journal of the American Ceramic Society*** **2008**, *91*, 1653-1658.

(21) Kang, Y. C.; Park, S. B.; Lenggoro, I. W.; Okuyama, K. ***Journal of Materials Research*** **1999**, *14*, 2611-2615.

(22) Guo, B.; Harvey, A.; Risbud, S. H.; Kennedy, I. M. ***Philosophical Magazine Letters*** **2006**, *86*, 457-467.

(23) Andrievskaya, E. R.; Zaitseva, Z. A.; Shevchenko, A. V.; Lopato, L. M. ***Inorganic Materials*** **1997**, *33*, 390-393.

(24) Porter, D. A.; Easterling, K. E. ***Phase transformations in metals and alloys*****; Van Nostrand Reinhold: New York, N.Y., 1981.**

(25) Hao, J. H.; Studenikin, S. A.; Cocivera, M. ***Journal of Luminescence*** **2001**, *93*, 313-319.

APPENDIX A

METHOD OF PARTICLE SIZE DISTRIBUTION MEASUREMENT USING TEM IMAGES

(a) Multiple TEM images are obtained randomly from each sample.

(b) The diameter of a particle is measured in random orientations on the TEM images.

(c) Each size bin is divided by 50 or 100 nm.

(d) The number of particles is counted for each bin.

(e) The number fraction is calculated for each bin.

(f) The particle size distributions in terms of number fraction are plotted with respect to the bin.

APPENDIX B

PHOTOLUMINESCENCE MEASUREMENT USING TB INTERNAL STANDARD

There are two kind of terbium oxide; one is Tb_2O_3 which has a photoluminescence property and the other is Tb_4O_7 which has a magnetic property with weak photoluminescence property. Tb_2O_3 is formed at high flame temperature (H_2 flame with O_2 support) while T_4O_7 is formed at low flame temperature (H_2 flame with Air support).

To prepare photoluminescence samples, 2.5% Tb-doped Y_2O_3 particles were used. The particles were synthesized at H_2 flame with O_2 support, using the same method (flame spray pyrolysis) which was used in this thesis. Figure 10. shows the photoluminescence spectra for 2.5% Tb-doped Y_2O_3 particles which were prepared in both H_2/O_2 and H_2/Air flame, with an excitation wave length of 230nm. The photoluminescence spectra matched well with Hao's results [25].

(a) Tb-doped Y_2O_3 is prepared as internal standard (internal standard should have the main peak which is not overlapped with spectra of target materials).

(b) Target material (Y_2O_3:Eu) and internal standard (Y_2O_3:Tb) are put together into a glass vial (5ml), holding the mass ratio of 1: 5~7.

(c) Isopropanol is added into the vial that contains the powder.

(d) The vial with the powder and isopropanol is sonicated for 30 min in ultra sonication vessel.

(e) Several drops of the particle suspension are dropped into a cuvette (OpticsPlanet, Inc., Northbrook, IL) and dried in room air.

(f) The bottom portion of the cuvette is cut down with a hacksaw, yielding a square plate that is approximately 3 mm tall. See Figure 11.

(g) Photoluminescence measurement is carried on fluorescence spectrophotometer using mixed and dried powder.

(h) Record the photoluminescence spectrum from 400nm to 700nm using 260nm excitation wavelength.

(i) The spectra of all samples are normalized at 488nm which is the main peak of Y_2O_3:Tb. Suppose the photoluminescence intensity at 488 nm is I_{488}, and the intensity at any given wavelength is I, then the normalized intensity is $I_{norm}=I/I_{488}$.

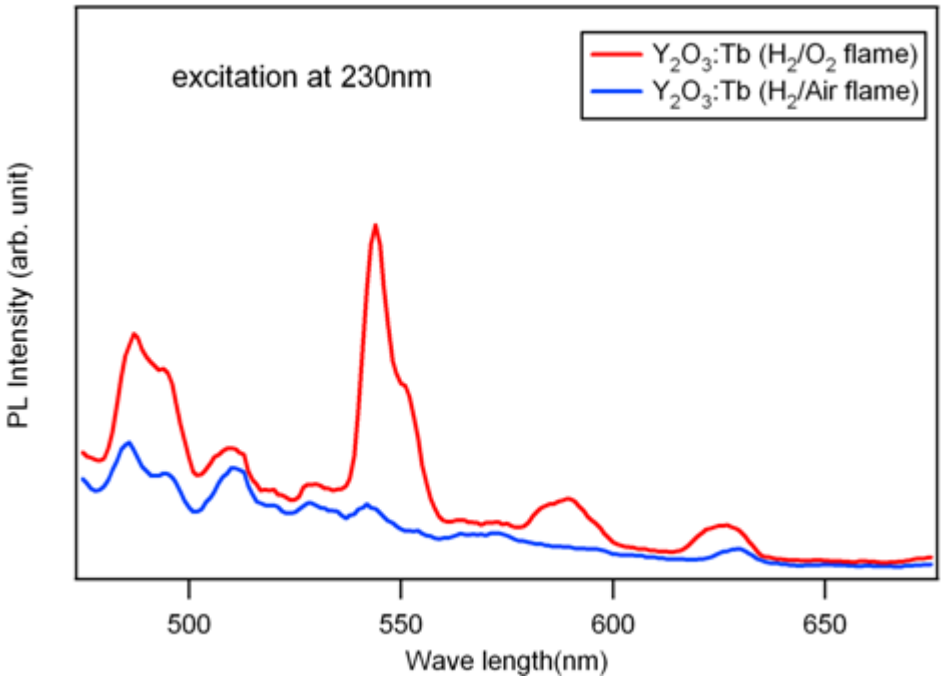

Figure 10. Photoluminescence spectra for Tb-doped Y_2O_3.

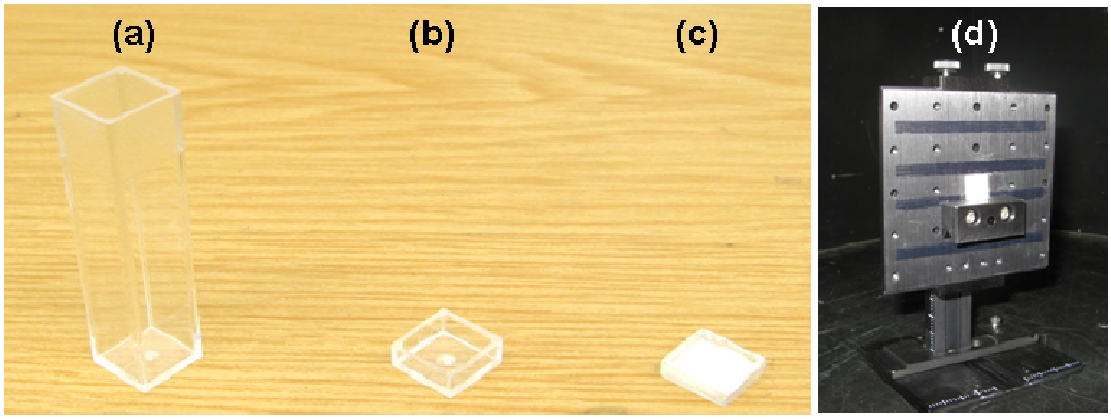

Figure 11. Preparation of photoluminescence sample. (a) cuvette (b) cuvette cut (c) mixed and dried powder on cuvette cut (d) cuvette cut on sample stage.

APPENDIX C

METHOD OF XPS DATA ANALYSIS USING SOFTWARE PROVIDED BY MANUFACTURER

(a) Go to the Vision Processing window by clicking on the Process bar at the bottom of the screen. If the Vision Processing window is missing on the screen, right click on the background and choose Programs and then Vision Processing with the left button. The Vision Processing window will pop-up within a minute.

(b) Click on File in the top left corner and choose Open Dataset for Processing. You should see the dialog window Open For Processing Data pop-up on the screen. Load your files, and the black data rectangles should appear at the bottom section of the Vision Processing window.

(c) Highlight the files that you want to check by left-clicking. Then by right-clicking, open the options box and choose the Processing option by left-clicking – the Processing window should pop up on the screen.

(d) Choose Quantify in the top row and you will see the spectra for all files that were highlighted in the Vision Processing window.

(e) At the top left-hand corner of the Processing window click on Options and choose Element list. This will bring up a display of elements and their respective binding energies. By clicking on the peaks and element position in both windows you can determine which elements are present in your spectra. When you are finished, click the middle button of the mouse to clear all lines.

(f) In the Quantification region of Processing window, enter an element and its most intensive photoelectron transition (e.g. O 1s) in each line of the table. Press Return. Using left and right mouse buttons zoom in on this area of the spectrum and make corrections to the borders as desired.

(g) After you have typed in all the relevant elements and corrected the quantification intervals for them, click Apply at the bottom of the Processing window.

(h) Go to the Vision Processing window and click on Options, then on Browser Actions commands. The Browser Actions window should appear on the screen. You should activate the Profile spectra option at the top. In each section below choose and highlight in the following order: Region- Area-Position-Position name- None, then click “Display window” at the bottom. The quantification report window should pop up on the screen.

VITA

Name:	Hoon Yim
Address:	19/10 81 Dangsan 2-Ga, youngdeungpo-Gu, Seoul, South Korea
Email Address:	yimhoon@hotmail.com
Education:	B.A., Materials Science and Engineering, Ajou University in South Korea, 2001 M.S., Materials Science and Engineering, Texas A&M University, 2009